

Mixing-induced aggregation and associated microstructures in the capillary flow

Steven Henck, Eric Treacy, and Jie Yang

Physics Department, University of Vermont, Burlington, Vermont 05405, USA

(Received 24 March 2009; published 18 August 2009)

With a device that uses microscopic imaging as the signal detection method for online laser light scattering of solutions driven to flow in a capillary tube, we have found that mixing of a solution with water and vice versa induce large numbers of aggregates in the free flow stream. The degrees of aggregation as measured from the total number of aggregates and the corresponding light-scattering intensities are dependent on the species of the solution. This species dependence of the mixing aggregation in the capillary flow has the potential for the development of new protocols or even spectroscopic methods for the detection of solute molecules and the assessment of solution qualities. Furthermore, even with pure-distilled and de-ionized water in the steady-state capillary flow, there are still countable numbers of aggregates detectable in the free flow stream, although of extremely low concentration of an estimated value of no more than 10^{-15} M.

DOI: [10.1103/PhysRevE.80.026306](https://doi.org/10.1103/PhysRevE.80.026306)

PACS number(s): 47.51.+a, 47.55.db, 47.61.Ne, 68.05.Cf

I. INTRODUCTION

Laser light scattering has wide applications for its nondestructive detection of soft matters in solutions [1–7]. Optical microscopy has long been substantial to reveal microscopic structures of a wide range of matters [8–10]. Thus, it can be expected that the combination of the two instruments will be particularly useful in applications involving detections and characterizations. A newly developed setup combining the laser light scattering and microscopic imaging has shown some initial successes for the online detection of proteins through the capillary gel filtration, yielding the detection sensitivity on the same order as that by conventional laser light-scattering instruments and showing the potential of improvements to the detectability [11].

One surprising feature revealed with microscopy is the dominance of “particlelike” structures in the capillary flow associated with the scattering intensity peaks in the gel filtration runs that would elude detection with conventional scattering instruments [12–16]. In particular with the present studies, we have found that there were countable particles even with pure-distilled and de-ionized water in the flowing stream. It has been known that there are always dissolved gases in water, typically on the order of 10 mg/L [17–19]. It might be possible that part of dissolved gases would form microbubbles and that would result in scattering entities seen as particles under the microscope. However, free microbubbles in water collapse from the inward pressure due to the surface tension, where a spherical bubble with the diameter of a micrometer has a lifetime of about a microsecond [20]. In this scenario, stable “free particles” in the steady-state free flow observed in our studies cannot be microbubbles.

In addition, the air concentration in the bubble is on the order of g/L, much larger than that of the dissolved air in water. Thus, at equilibrium, the generation of bubbles in water is not favored. This is the reason in sonoluminescence experiments, not only external ultrasound radiation has been used but also the choices of various gases surrounding the water have been attempted [21]. Under a different circumstance, if the pressure is decreased by pumping on a water

surface, large air bubbles with radii much larger than a micron can be seen by naked eyes. They float to the top of the water rather than collapsing. Visible air bubbles are also often seen tethered to glass or plastic walls, quite stable. However, these bubbles will detach from the tethered surface and float upward once agitated. There is a big difference between a free-standing bubble and a bubble tethered to a solid surface. Note that bubbles that cause problems in gel filtration or high pressure liquid chromatography (HPLC) columns are big ones as they literally block the solution flow path (or choke the flow path) while the column packing materials provide numerous surface areas to tether these bubbles [22–24]. Thus, micrometer size free bubbles collapse and large free bubbles move up.

From a different perspective, we note that even for pure-distilled and de-ionized water, there still are impurities such as ions and small molecules. The water quality is considered very good if the impurity contents are less than one part per million [25,26]. Yet according to the molecular perspectives, one part per million still represents a very significant total number on the order of 10^{17} molecules per liter. If these impurities, in particular, charged ones such as ions, form aggregates, an aggregate can result in a giant electric dipole to be a very strong light-scattering entity. It has been well established that the probability to form such aggregates should be very small in thermal equilibrium for most impurities except amphiphilic molecules according to statistical thermal physics [27–30].

We have modified the setup that has shown initial successes in the detection of proteins, with the key modification being to allow direct laser light transmission. Using the modified setup, we have discovered that mixing of a solution with water and vice versa induce large numbers of aggregates in the free flow. The mixing was generated as a buffer solution was replacing pure water and vice versa in the capillary flow. The linear flow speeds in our experiments were far below that for the onset of turbulence [31,32]. These mixing-induced aggregates persisted over tens of minutes in free solution after the flow was stopped. The degrees of the mixing aggregation as measured from the total number of aggregates and corresponding light-scattering intensities showed a clear dependence on the species of solutes (mostly

ions). This species-dependent mixing aggregation reflects intrinsic interactions between dissolved molecules and poses the potential for future developments of new protocols or spectroscopic methods for the detection of molecular solutes and the assessment of solution qualities.

II. BASIC THEORIES AND INSTRUMENTATION FUNDAMENTALS

Free microbubbles in water. It is possible that dissolved gas molecules can form free microbubbles in water. However, the lifetime for a free gas bubble in water is very short because of a rather large collapsing pressure due to the surface tension of water. The collapse of a free spherical bubble of radius R is governed by the well-established Rayleigh-Plesset equation [21]. Accordingly, neglecting the viscous effect of water, we have

$$2\rho_w R^2 \frac{d^2 R}{dt^2} = -3\rho_w R \left(\frac{dR}{dt} \right)^2 - 4\gamma, \quad (1)$$

where γ is the surface tension of water at the air-water interface, about 80 mN/m at room temperature [33,34], dR/dt is the radius changing rate, d^2R/dt^2 is the radial acceleration, and ρ_w is the density of water. This equation is consistent with a negative changing rate of the radius due to the collapsing of the bubble. On this basis, we can estimate the order of magnitude of the lifetime of the bubble. The approximate lifetime τ is determined by the following equation:

$$\tau^2 \sim \frac{\rho_w R^3}{\gamma}, \quad (2)$$

giving a lifetime on the order of a microsecond for a free bubble of the radius of a micrometer. Thus, the lifetime for free air bubbles of radii of microns or less in water is on the order of microseconds or less, consistent with earlier studies [20]. Note that a bubble attached to a solid substrate may have a much longer lifetime because of possibly favorable boundary interactions to stabilize the tethered bubble.

If one includes the viscous dragging force, there is an additional term of $(-8\eta dR/dt)$ to be added to the right-hand side of Eq. (1), where η is the viscosity coefficient of water. We can do an order-of-magnitude estimate to see if the viscous term is important. For pure water, the viscosity coefficient of water at room temperature is 10^{-3} Pa s. For R , about 1 μm and, for t , about 1 μs , dR/dt is about 1 m/s. This gives $8\eta dR/dt$ of about 8×10^{-3} N/m. The term 4γ has a value of about $4 \times 80 \times 10^{-3}$ N/m. Thus, the viscous term is much less important so it is a good approximation to neglect it. We also neglect an external force term in the above treatment. This term adds a constant pressure to the bubble if the size of the bubble is small enough. Such a constant pressure would not affect the bubble dynamics.

Statistical physics of aggregation in thermal equilibrium. The aggregation of solute particles (molecules) has been well studied in systems containing micelles. The key feature is that the concentration of particles in aggregates of N particles can be dominant if the Gibbs free energy for each particle in

the aggregate can be smaller than that for a free particle according to the following [27–29]:

$$X_N = N \{ X_1 \exp[(\mu_1^0 - \mu_N^0)/kT] \}^N, \quad (3)$$

where X_N is the concentrations of particles (not aggregates) in the N -particle aggregates and X_1 is the concentration of free individual particles, μ_N^0 and μ_1^0 are corresponding Gibbs free energies per particle, and kT is the thermal energy per particle. For noninteracting free particles, the chemical potentials μ_N^0 and μ_1^0 are approximately the same so that the concentration of particles in N -particle aggregates should be extremely small. This is a case in which the probability to form the N -particle aggregate in the system is accordingly much less than one. If there is an attraction between particles, the chemical-potential energy per particle can be smaller for a particle in the N -particle aggregate than that as a free one ($\mu_N^0 < \mu_1^0$). Typically, in this case there is a critical concentration of particles and above which aggregates are favored, as the case of critical micelle concentration in systems containing amphiphilic molecules, such as detergents, etc. [27,29].

Note that the concentration of aggregates is fixed in thermal equilibrium, albeit with very small value if μ_N^0 is not much smaller than μ_1^0 . Thus, accordingly, the lifetime of aggregates on average should be very long or infinite. However, for any given aggregate, the equilibrium is dynamic, with an equal number of molecules leaving the aggregate as that joining the aggregate. Yet in nonequilibrium environments, such as in regions of apparent concentration gradients, where the mixing process is ongoing with accompanying constant solution flow, an understanding of the underlying mechanism governing the aggregation probability is still lacking. Our experimental results do indicate the dominance of the mixing-induced aggregation.

Optical imaging and light scattering. The coupling of microscopic imaging, laser light scattering, and the capillary flow has been essential for our discovery of the phenomenon of the mixing-induced aggregation in the capillary flow. Because of the unique three-way combination in our setup, it is important to discuss briefly the essence of the involved optics and the signal detection schemes.

According to the principles of geometric optics, there is a one-to-one mapping between an object and an image with the microscope. In Fig. 1(a) we use a single lens to avoid the complication of the multiple lens assembly of a microscope objective lens yet still retain the physics of the ray optics. In contrast to popular cameras for picture taking, in the microscope an object must be located at a plane—often referred to as the object plane—in order to form a real image at the detector plane where the charge-coupled device (CCD) chip is located [35]. The area of the CCD chip determines an object area such that if a point within the object area scatters light, it results in a bright imaging spot at the chip. The brightness (or intensity) of the imaging spot is proportional to that of the original light-scattering point.

The detection of scattered light with conventional light-scattering instruments has a different feature from that with a microscope. With the typical scenario of conventional light scattering [Fig. 1(b)], there is a scattering site and the vol-

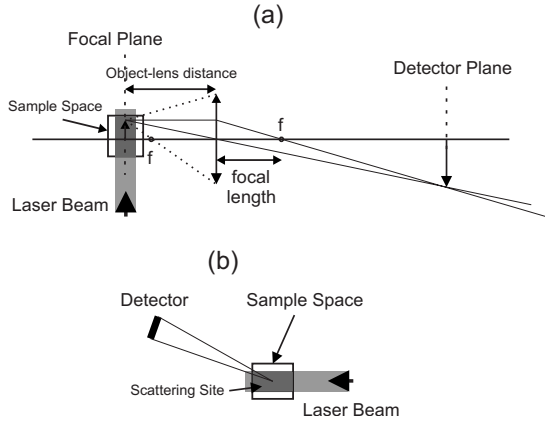


FIG. 1. Two illustrations of light-scattering detection schemes. Part (a) shows a typical ray diagram of a single lens microscope with light collection through imaging and part (b) demonstrates the detection scheme with conventional instruments. In part (b), the entire dark shaded volume in the sample space is the scattering site. In part (a), only a small portion of the shaded volume, the objective plate, is the scattering site. In both cases, the sample space is larger than the volume swept by the laser beam to avoid scattering from boundary solid materials (in our case, the glass wall of the guiding tube).

ume of which is the cylindrical volume swept by the laser beam in the sample space. For a point particle in the scattering site that scatters light, only a very small fraction of scattered lights reaches the detector. This fraction is proportional to the small solid angle subtended by the detector to the particle.

With the microscope, the scattering point at the object area is subtended a rather large solid angle by the aperture stop of the objective lens. Moreover, all scattered light rays after the lens converge to the imaging spot on the CCD chip at the detector plane. However, if the scattering point is off the object plane, the light intensity profile at the detector plane differs dramatically from that with the scattering point on the object plane. Neglect the block of light by the aperture stop and assume the ideal ray optics [35,36], the normalized intensity distribution function at the detector plane for the off object plane scattering is of the form

$$f(r) = \frac{1}{4\pi} \frac{d}{(d^2 + r^2)^{3/2}}, \quad (4)$$

with

$$\int_0^{2\pi} d\varphi \int_0^\infty f(r) r dr = \frac{1}{2}, \quad (5)$$

where d is the distance from the imaging spot to the detector plane, r is the distance to the origin of coordinates on the detector plane, and $rdrd\varphi$ is the surface integral element of the cylindrical coordinates on the detector plane. The origin of coordinates on the detector plane is the point of intersection by a line through the plane. This line is parallel to the optical axis and runs through the imaging spot and the detector plane. The resulting half in Eq. (5) is because the detector plane is at one side of the point object. Note that

$f(r)|_{d=0}$ is one half of the two-dimensional Dirac delta function. The intensity at the origin decreases rapidly as d increases.

In reality, the nature of wave optics also plays a role. Thus, the effective region for light collection with the microscope is not just a planar area but rather a thin plate of the area that of the object area and the thickness on the order of the wavelength. We refer this effective light collecting volume as the object plate on the basis of geometric and wave optics. For light scattering, this object plate is the scattering site, much smaller than the volume swept by the laser beam through the sample space. Note that the scattering by a point off the object plate does not form a sharp image on the CCD chip and thus does not contribute much to the detected light intensity. It is surprising that such a dramatic reduction in the volume of the scattering site has not led to any significant reduction in the detectability. Since the detection sensitivity with the CCD camera is not really any better than that with light detecting elements in conventional light-scattering instruments, the imaging formation focusing scheme must be the major factor to compensate the significant lose of the light collecting volume to result in the extremely high detection sensitivity comparable to that with conventional light-scattering instruments.

More importantly, rapid developments in semiconductor industry have made high power lasers readily available and CCD cameras extremely sensitive imaging tools [37]. In particular, intensified CCD cameras have capabilities to detect light at extremely low levels, capable of sensing light emitted from a single fluorophore, evidenced by recently emerging single molecule experiments [38–42]. Therefore, there are bright future perspectives to yield much higher detection sensitivity by the combination of the laser light scattering and microscopic imaging in capillary flow devices.

III. MATERIALS AND METHODS

Materials. All salts and stock buffers were obtained from Sigma. All buffers and salt solutions for our experiments had neutral pH values. They were either diluted from stock buffers or prepared in the lab with distilled and de-ionized water. Powders of α -D-glucose were obtained from the Chemistry stockroom at University of Vermont.

Instruments and devices. High power handheld lasers were obtained from LaserGlow (Toronto, Canada) and powered by a power supply. An intensified CCD camera (IC-110 from PTI, Monmouth, NJ) mounted on a Nikon Optiphot 2 microscope was used for the imaging and the detection of the scattered light intensity. The amplitude detector was assembled in the lab according to the standard circuit diagram [43]. Voltmeters with the IEEE interface were used to record the output from the amplitude detector.

The major scheme of experimental setup. The modified detection setup was similar to the prototype device used earlier in the capillary gel filtrations runs [11]. The major difference was that this setup did not use the capillary L-tube. Instead, the laser beam was directly transmitted to the sample space through a needle with a glass window at the tip, as shown in Fig. 2(a). The laser needle was embedded in

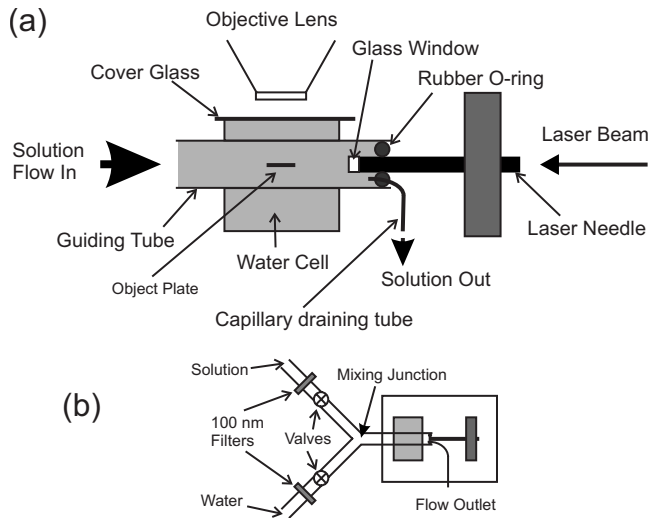


FIG. 2. Sketches of the detection setup (not in proportion to the real setup): (a) details around the object plate and (b) the capillary flow scheme. Major pieces, key functional sites, the incident laser beam location, and the capillary flow schemes are labeled to show general operational principles of the setup.

an aluminum block to ensure mechanical stability. The glass window was glued on with epoxy. This window allows direct laser transmission, preserving the laser collimation.

The guiding tube was the same kind (of flint glass) used in the earlier setup and was coupled to the laser needle with a soft rubber o-ring for waterproof. The tube was placed in a water cell with the objective lens of the microscope on top of the cell. The object plate was inside the guiding tube just off the laser needle window, as depicted in Fig. 2(a). A capillary draining tube was pierced through the rubber o-ring for the continuous flow of solutions through the guiding tube. The solution was directed to flow toward the needle in normal runs.

The water cell and the thin-wall guiding tube are essential to minimize image distortions. The image distortion is prone to occur as light rays that enter the microscope must first shine through materials of different indices of refraction and corresponding interfaces of various surface curvatures. Severely distorted images of light-scattering objects will occur if a thick wall guiding tube is used or the imaging of the guiding tube interior space is directly through air without the water cell.

A major effort in the assembly of the setup was to minimize stray lights into the microscope objective lens. The guiding tube needed to be properly aligned to avoid the transmitted laser beam from directly hitting the tube. It is critical that the glass window is clean and free from any epoxy residue because the scattering from any object on the window can hit the guiding tube to result in a very bright background.

The capillary flow. Our experiments were done at room temperature ($\sim 23^\circ\text{C}$) with the capillary flow driven by the gravity. There were two reservoir bottles (not shown in Fig. 2), one for water and the other for solutions, with both placed higher than the draining capillary tube. Figure 2(b) shows the mixing scheme in the setup immediately adjacent to the de-

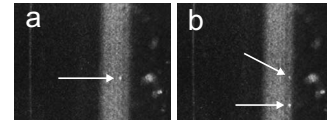


FIG. 3. Two snapshot images of pure-distilled and de-ionized water in the capillary flow. Arrows point to moving aggregates caught by the snapshots. Image area for each: $2.4 \times 1.8 \text{ mm}^2$.

tection unit. The two valves were placed close to the sample space and the net length of capillary tubes, including the guiding tube, was about 10 cm from the mixing junction to the laser needle window. The capillary flow had a volume flow rate of 0.045 ml/min. On the average, the linear flow speeds for our runs were in the range of 0.6–0.9 mm/s, corresponding to normalized Reynolds numbers of 1.1–1.9, far below that for the onset of turbulence [31,32]. In our experiments, the pure water was typically used for less than three days and then we filled the water bottle with new water for consistency. All solutions used were first filtered through a 200-nm-filter membrane before loading to the solution bottle. In addition, a filter membrane of pore size of 100 nm, as shown in Fig. 2(b), was used immediately before each valve to prevent any large object from flowing to the scattering site. We tried a degassing procedure where a bottle of water and a bottle of 100 mM Tris chlorine (TrisCl) were pumped for about 10 min to let gas out. Then, these bottles were placed at their normal positions for the mixing flow run. The results with these degassed bottles were similar to those without the degassing procedure. Thus, in our routine experiments, the degassing procedure was not employed.

For a mixing flow run, the water valve was opened to let steady flow to establish and to flush out the guiding tube. Then, the water valve was closed as the solution valve was opened. The solution flow was allowed to reach steady state as seen from the monitor screen and the intensity recording curve. After which, the flow was switched back to water. These back and forth switches were done several times until the shown intensity curves gave the similar features.

IV. RESULTS

Microscopic structures in the steady-state capillary flow of water and solutions. For distilled and de-ionized water in the steady-state capillary flow, there were still countable numbers of bright spots in the stream after the 100-nm-filter membrane. Figure 3 shows two snapshot images with part (a) one spot and part (b) two spots marked by arrows. There were also snapshots without any aggregate and ones with more aggregates. In one trial with the distilled and de-ionized water, a total of 661 spots were seen to flow through the field of view in 18.6 min. Typical linear speed of these flowing spots was less than 1 mm/s. Thus, on average, there were about one to two spots on the monitor screen every 2 to 3 s. Note that a spot represented a strong scattering center but its actual size could be much smaller, similar to the case with single molecule experiments, where the light source was from a single molecular fluorophore, but the image size of the corresponding bright spot seen with the microscope was on the order of micrometers [38].

TABLE I. Linear flow speeds of bright spots in the steady-state flow of solutions and water.

Species	Speed (mm/s) (10)	Normalized Re number
Glucose	0.84 ± 0.12	1.7
	0.84 ± 0.08	1.7
Na_2HPO_4	0.78 ± 0.03	1.6
	0.56 ± 0.14	1.1
KCl	0.73 ± 0.05	1.5
	0.57 ± 0.05	1.1
CaCl_2	0.78 ± 0.07	1.6
	0.73 ± 0.05	1.5
NaCl	0.72 ± 0.02	1.4
	0.76 ± 0.05	1.5
AF	0.95 ± 0.12	1.9
	0.93 ± 0.03	1.9
MOPS	0.86 ± 0.09	1.7
	0.89 ± 0.04	1.8
TrisCl	0.90 ± 0.03	1.8
	0.88 ± 0.03	1.8
TrisP	0.92 ± 0.04	1.8
	0.95 ± 0.04	1.9

Countable bright spots were also present in the steady-state capillary flow of solutions. The linear flow speed of a moving bright spot could be measured from the corresponding video clip. Table I summarizes the linear flow speeds of bright spots in the steady-state flow of solutions and water. The middle column shows the average flow speed with the standard deviation and the right column is the corresponding normalized Reynolds number. For each species, the upper row is the average speed taken in the region where the steady-state flow for the solution was reached and the lower row is that for the water after the switching back. Each average was from ten measurements. Spots on the screen were not at the same radial position. Thus, it is not surprising to see large standard deviations in some measurements because according to the fluid mechanics of the lamellar tubular flow, the linear speed inside the tube has a quadratic functional dependence on the radial distance from the central axis [44].

The mixing aggregation. The most surprising finding in our studies has been the generation of huge numbers of spots as a solution is mixing with pure water and vice versa. Figure 4 shows light-scattering intensity curves that summarize the main feature of this phenomenon. Each curve represents a typical run for the labeled solution species. For all intensity curves, the first peak is due to the replacing of the water flow with the flow of a solution and the second peak is from the switching back to the water. For the water run, the switching was between two reservoirs of water. The water run is the control and it shows that the mixing is indeed the factor to generate large numbers of aggregates and large scattering intensity peaks. The base and starting time for each curve have been arbitrarily shifted to show the main feature of each curve. There are three base lines in the figure: the original

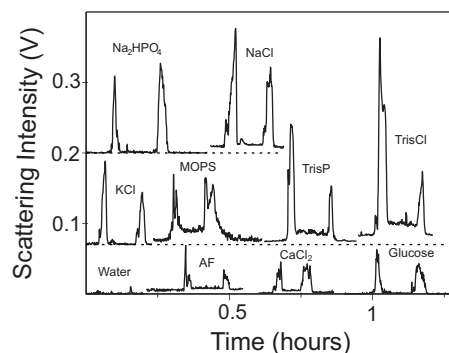


FIG. 4. Light-scattering intensity curves with the horizontal axis in hours and the vertical axis in volts. The voltage is the direct reading of the video output by the amplitude detector and is proportional to the detected light intensity, but the conversion factor has not been calibrated. Thus, these curves represent relative measurements of the scattering intensities. The name (or abbreviated one) above each curve labels the solution species in the mixing run through the capillary flow. The two shifted base lines above the original one are marked by dashed lines. Six solution curves have been shifted linearly in both base and time to avoid curve overlapping. No base shifts were made for the water, AF, CaCl_2 , and glucose curves.

one ($V=0$) and the two shifted bases indicated by the horizontal dashed lines in the figure.

In our experiments, each curve was yielded after several mixing runs until the first and second peaks consistently repeated the same features between runs. For different solutions, the number of runs varied somewhat but they were in the range of four to seven times. Sample preparations were slightly different for different solutions. The TrisCl buffer was 100 mM, diluted from a stock buffer of 1 M, pH 8. The tris phosphate (TrisP) buffer was 80 mM, diluted from a stock buffer of 0.8 M, pH 7.4. The other three buffers ammonium formate (AF), 3-(N-morpholino)propanesulfonic acid (MOPS), and sodium phosphate (Na_2HPO_4) were prepared from dried powders to a final concentration of 100 mM and adjusted to neutral pH values. In order to maintain the neutral pH value, NaCl, KCl, and CaCl_2 solutions (all of 100 mM) were prepared with 4 mM AF. The glucose solution (100 mM) was prepared with distilled and de-ionized water without any buffering attempts.

In addition to the general features of the mixing aggregation, possibly driven by the concentration gradient, another characteristic feature is that the degrees of aggregation as measured from the light-scattering intensity and the total number of aggregates are species dependent. According to these intensity curves, the first peak of the TrisCl curve stands out the highest of the nine species. The sodium phosphate (Na_2HPO_4) buffer gives the largest second peak. For some curves, the water background is above the base, indicating stronger background scattering in those cases. The stronger background scattering could be due to stray light scattering from objects on the laser needle window. It was critical in these cases to optimize the position of the guiding tube, where any slight misalignment would cause a much larger background scattering. Thus, it was essential to optimize the guiding tube alignment with respect to the laser

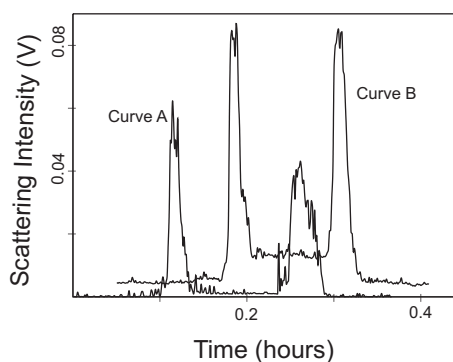


FIG. 5. Curves A and B are two scattering intensity plots correspond to two runs with the 100 mM glucose solution by two different laser needle windows. Curve B has the time shifted to avoid overlapping of main features of the two curves. No base shift for both curves.

needle; but in practice, the involved adjustments often were time consuming and rather frustrating. The optimal approach was yielded after devoting great efforts to clean off any objects on the window. If the cleaning was successful, it became relatively easy to align the guiding tube because of the superb collimation of the laser beam and that the transmitted beam diameter was the same as the inner diameter of the laser needle, whereas the guiding tube's inner diameter was larger than the outer diameter of the laser needle.

There is also a distinct feature that depends on the species of the solution. The steady-state background scattering by the solution could be a step higher than that by the water. This step is likely due to the classical molecular dipolar scattering by solute molecules [1–3]. Note that this effect is more prominent with those curves that already have shown a higher than the base level steady-state water background. With the water background at the base, the glucose curve has a smaller step rise than that with the CaCl_2 curve, whereas neither the KCl curve nor the Na_2HPO_4 curve has any detectable step.

Figure 5 shows two glucose running curves by different laser needle windows with one curve of a higher water background. Both curves show the step feature with the curve B of higher water background having a larger net step rise. Although details of the curves are not the same, major structural characters of the two runs are very similar. In the plateau regions, any snapshot either shows the passing of a few bright spots or nothing at all. At the rising and falling tails of any peak for both curves (below half of the peak), there are roughly even distribution of aggregates. Images (a) and (b) in Fig. 6 were taken at the rising tails of the first peak of curves A and B, respectively. Note that these aggregates actually could be distributed in the entire guiding tube but only those in the region shined by the laser beam were seen in the images. The peak regions, with the glucose peaks smaller ones among all species studied here, show characteristic large bright spots, possibly due to an overlapping of a number of aggregates. Figures 6(c) and 6(d) are images at the first peak of curves A and B, respectively.

Microscopic structures of aggregates. In fact the mixing aggregation bares the similar microscopic structural features

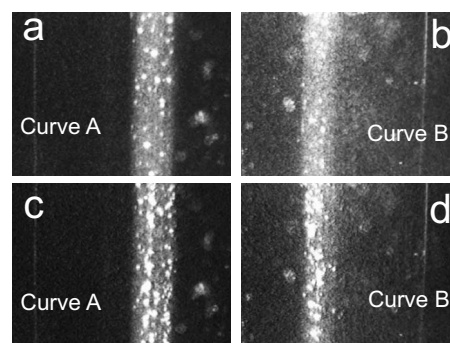


FIG. 6. Snapshot images correspond to the two runs in Fig. 5. Images (a) and (b) were taken at the rising tails about one quarter of the maxima of the first peak of curves A and B, respectively. Images (c) and (d) were taken at corresponding maxima. Image area for each: $2.4 \times 1.8 \text{ mm}^2$.

for all nine species in our studies, with roughly even distribution of aggregates as the peak develops and fades, corresponding to the rising and falling tails of the peak but showing larger spots at the peak. These spots at the peak would sometimes become very large and numerous and a thick white line would appear. Figure 7 shows representative images corresponding to snapshots taken either at the rising tail or at the peak for four species. There is a characteristic thick white line for KCl and Na_2HPO_4 curves at the peak, a not so bright line for the CaCl_2 peak. The TrisCl peak is so strong that the entire laser beam region becomes bright white. The bright white stripe at the peak must be due to the overcrowding of aggregates so that the scattering from individual ones overlap and overlaying on each other.

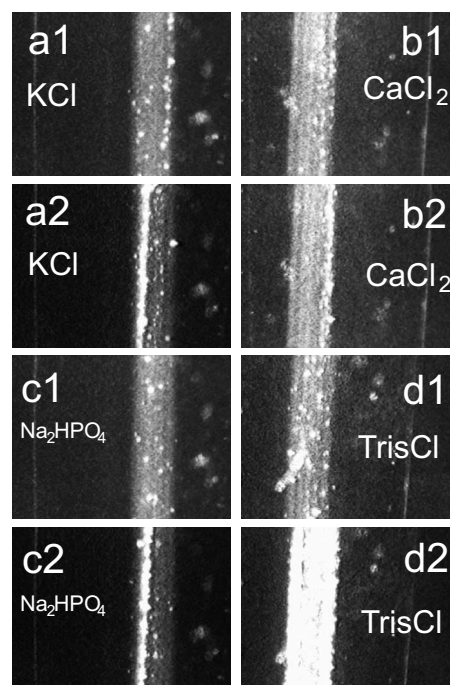


FIG. 7. Here are eight representative images taken along the rising tails and at top regions of the first peak for four species. Image area for each: $2.4 \times 1.8 \text{ mm}^2$.

An interesting experimental condition is also revealed from these images in Fig. 7. Accordingly, the KCl and Na_2HPO_4 curves were taken with a laser needle window of minimal stray lights and the CaCl_2 and TrisCl runs used a window with more stray lights and thus higher background scatterings.

V. DISCUSSION

According to the volume flow rate of water and the measured number flow rate of aggregates, also taking into account of the fact that the microscope only maps an object plate of a volume with the thickness about the wavelength of the light source and the area (object area) of several square millimeters, we can estimate the concentration of aggregates in pure water. Under an optimum assumption that what we observed under the microscope was part of a uniform distribution of aggregates over the entire volume of the guiding tube of an inner diameter about 2 mm, the maximum concentration for aggregates in pure water was about 10^9 /liter. For a concentration of 1 M of a species, the net molecular number per liter is the Avogadro's number of 6.02×10^{23} . Thus, the estimated maximum aggregation concentration in water was about 10^{-15} M.

It is amazing that our setup can yield such astonishing detection sensitivity but we note that this achievement is possible mainly due to the fact that these aggregates are strong scattering centers. In fact, the aggregation concentration will certainly be still lower because some spots can be due to contaminants. Aggregates in the steady-state flow belong to aggregates in thermal equilibrium. Therefore, it is consistent to have the extremely low aggregation concentration because of the correspondingly very low aggregation probability, in contrast to cases with micelle systems [27].

Note that according to the scattering intensity curves in the steady flow, the passing of these countable scattering centers does not show any unambiguous signal above the noise level of the background, as seen from both Figs. 4 and 5. Thus, the imaging method gives superior detection sensitivity because these scattering centers are clearly seen moving across the monitor screen.

The most important finding is the mixing-induced aggregation. The mechanism of the aggregation is not clear at present. In our case, there were constant flow and ongoing processes of mixing, so that the systems were not in thermal equilibrium. The aggregation formalism in thermal equilibrium does not apply here. Nevertheless, these aggregates have been stable over a long time, basically ruling out the scenario that any free gas (air) bubbling mechanism can be responsible for the observed phenomenon.

The long-time stability of free aggregates in solution is evidenced from stop flow runs. In one trial, it was shown that after stopping the flow the mixing aggregates did not show any sign of fading or decaying as the solution remained stationary in the guiding tube for a long time. Figure 8 shows the trial with 100 mM TrisCl, where the flow was stopped as the first peak was rising near its maximum. These aggregates persisted for a period of more than 10 min and showed no sign of any decaying as the flow was paused. Furthermore,

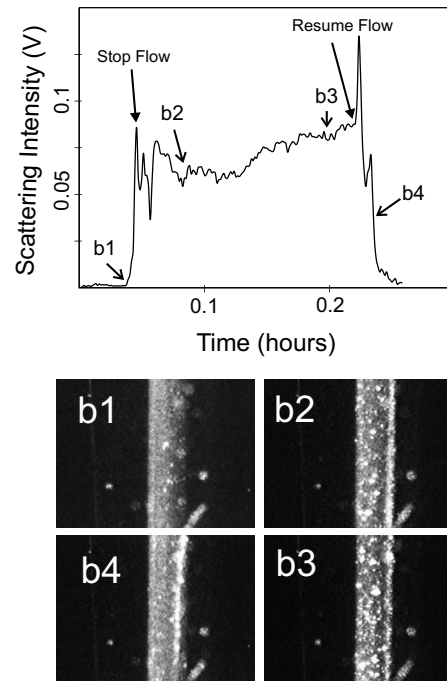


FIG. 8. The plot shown here is the scattering intensity curve taken in a stop flow run with 100 mM TrisCl, pH 8. The four snapshots were taken at corresponding points marked on the curve. Fixed spots in these images are likely objects attached to the guiding tube. Image area for each: 2.4×1.8 mm².

these aggregates were at the center of the guiding tube free in solution without contacting the solid glass tube wall. We did not try to monitor the aggregation structures for much prolonged time because the scattering intensities did not drift downward, as shown in the intensity curve. Actually, after the flow was stopped, aggregates inside the guiding tube were seen to slowly drift across the monitor screen instead of completely stationary. However, the overall total number of aggregates remained roughly constant, as reflected in the intensity curve shown here. Images b1–b4 in Fig. 8 were snapshots of microstructures at corresponding positions on the scattering intensity curve (marked by arrows). After the flow was stopped, there were lots of aggregates and roughly a white line at the right side of the laser beam region. The image b1 corresponds to the start of the first peak, with several aggregates seen in the area of the laser beam. Images b2 and b3 were taken while the flow was paused. The image b4 corresponds to a point on the falling tail after the flow was resumed.

This phenomenon indicates that the mixing aggregation in the capillary guiding tube can persist for tens of minutes or even longer. This appears to be at odds with our results of the steady-state capillary flow of solutions, where the net concentration of aggregates is extremely small ($<10^{-15}$ M). The extremely low concentration is consistent with the expected extremely low aggregation probability according to statistical physics at thermal equilibrium [27,29]. It must be the case that the mixing aggregation should eventually disappear once the equilibrium state is reached. For our system, the solution is inside capillary tubes, including the guiding tube, the draining tube, and the solution flowing tube connected to

the guiding tube. Thus, to reach equilibrium purely on the basis of diffusion can take very long time so that may be part of the reason there is no trend of aggregation decaying on the time scale of tens of minutes. Convection flow may also contribute to the reaching of equilibrium so that may be the reason of our observation of the drift of aggregates while the solution was stationary.

One possibility for the aggregates is the formation of droplets as the solution is in contact with water and vice versa. In this scenario, the surface free energy of the solution must be different from that of water. Then, the formation of droplets will be entropically more favorable because with the same interfacial free energy, the system of multiple droplets has a larger entropy than that of an interface separating two entities. Since solutions or water are incompressible, thus, unlike air bubbles, droplets can persist longer time until diffusion kicks in to smear out the boundary of droplets. Studies are still in need to sort out details to pin down the aggregation mechanism.

A note of caution worth mentioning here is that the average diameters of aggregates, as they appear to be of microns or larger, can be actually much smaller. This is due to the limitation of imaging and the nature of light scattering. With imaging, the smallest spot corresponds to the mapping of a pixel. In our case, with a CCD array of 640×480 pixels and mapping an area of 2.4×1.8 mm², each pixel represents an

object area of 3.5×3.5 μm². With the scattering, a bright spot, no matter how small it really is, shows up on the imaging screen of a minimal size of a pixel. By pure probability consideration, a bright spot is more likely to shine up several neighboring pixels because the imaging spot may not be squarely right at the center of 1 pixel. In addition, if several bright spots are in close vicinity then they may appear as one giant spot, which is of course not a true reflection of the situation at the object plate.

Although the mechanism of the mixing aggregation is not clear at the moment, the phenomenon itself offers the potential for the development of new spectroscopic methods and protocols for detection and characterization applications.

The modified detection setup uses a direct laser transmission that allows minimal stray lights, helping to reduce detection noise levels so that only the scattered lights of interest are detected and imaged. There is a potential to reduce the diameters of both the guiding tube and the laser needle for much smaller scale applications, possibly at nanometer scales for single molecule detection experiments.

ACKNOWLEDGMENTS

We thank Junru Wu for helpful discussions. Partial support from a UVM inventor pre-seed fund and a Vermont EPSCoR SBIR phase zero grant are acknowledged.

-
- [1] D. J. Sinclair, *J. Opt. Soc. Am.* **37**, 475 (1947).
 [2] W. Heller, *Rec. Chem. Prog.* **20**, 209 (1959).
 [3] P. J. Debye, *J. Phys. Colloid Chem.* **51**, 18 (1947).
 [4] G. Popescu and A. Dogariu, *Appl. Opt.* **40**, 4215 (2001).
 [5] W. Burchard, in *Laser Light Scattering in Biochemistry*, edited by S. E. Harding, D. B. Sattelle, and V. A. Bloomfield (Royal Society of Chemistry, London, 1992), pp. 3–22.
 [6] S. E. Harding, *Biotechnol. Genet. Eng. Rev.* **14**, 145 (1997).
 [7] W. Brown, *Dynamic Light Scattering: The Method and Some Applications* (Clarendon Press, Oxford, 1993).
 [8] S. Bradbury, *An Introduction to the Optical Microscopy* (Oxford University Press, New York, 1983).
 [9] T. Wilson, *Confocal Microscopy* (Academic Press, London, 1990).
 [10] W. Rodgers and M. Glaser, in *Optical Microscopy: Emerging Methods and Applications*, edited by B. Herman and J. J. Lemasters (Academic Press, San Diego, 1993), pp. 263–283.
 [11] J. Yang, *Anal. Chem.* **79**, 3881 (2007).
 [12] B. S. Kendrick, B. A. Kerwin, B. S. Chang, and J. S. Philo, *Anal. Biochem.* **299**, 136 (2001).
 [13] T. Wang and J. A. Lucey, *J. Dairy Sci.* **86**, 3090 (2003).
 [14] J. Wen, T. Arakawa, and J. S. Philo, *Anal. Biochem.* **240**, 155 (1996).
 [15] E. Folta-Stogniew and K. R. Williams, *J. Biomol. Tech.* **10**, 51 (1999).
 [16] J. A. P. P. van Dijk and J. A. M. Smit, *J. Chromatogr., A* **867**, 105 (2000).
 [17] A. H. Manning, D. K. Solomon, and A. L. Sheldon, *Ground Water* **41**, 440 (2003).
 [18] P. Nithyanandan, G. Deng, W. Brown, R. Manning, and S. Wahab, *Dissolution Technol.* **8**, 15 (2006).
 [19] B. J. Watten and D. R. Smith, *J. World Aquacult. Soc.* **28**, 316 (1997).
 [20] W. L. Nyborg, in *Encyclopedia of Applied Physics*, edited by George L. Trigg (VCH Publishers, New York, 1991), Vol. 2, p. 403–420.
 [21] M. P. Brenner, S. Hilgenfeldt, and D. Lohse, *Rev. Mod. Phys.* **74**, 425 (2002).
 [22] A. Weston and P. R. Brown, *HPLC and CE: Principles and Practice* (Academic Press, Cambridge, 1997).
 [23] D. Johns, in *HPLC of Macromolecules*, edited by R. W. A. Oliver (Oxford University Press, Oxford, 1989), pp. 1–42.
 [24] S. Mori and H. G. Barth, *Size Exclusion Chromatography* (Springer, New York, 1999).
 [25] M. A. Saleh, F. H. Abdel-Rahman, B. B. Woodard, S. Clark, C. Wallace, A. Aboaba, W. Zhang, and J. H. Nance, *J. Environ. Sci. Health, Part A: Toxic/Hazard. Subst. Environ. Eng.* **43**, 335 (2008).
 [26] Z.-G. Ji, *Hydrodynamics and Water Quality: Modeling Rivers, Lakes, and Estuaries* (Wiley-Interscience, Hoboken, NJ, 2008).
 [27] C. Tanford, *The Hydrophobic Effect: Formation of Micelles and Biological Membranes* (John Wiley & Sons Inc., New York, 1973).
 [28] J. N. Israelachvili, S. Marčelja, and R. G. Horn, *Q. Rev. Biophys.* **13**, 121 (1980).
 [29] G. Cevc and D. Marsh, *Phospholipid Bilayers: Physical Properties and Model* (Wiley, New York, 1978).

- [30] P. R. Cullis and M. J. Hope, in *Biochemistry of Lipid and Membranes*, edited by D. E. Vance and J. E. Vance (Benjamin, Menlo Park, 1985), pp. 25–72.
- [31] D. Greenblatt and E. A. Moss, *ASME J. Fluids Eng.* **125**, 1072 (2003).
- [32] B. Hof, J. Westerweel, T. M. Schneider, and B. Eckhardt, *Nature (London)* **443**, 59 (2006).
- [33] G. Roberts, *Langmuir-Blodgett Films* (Plenum Press, New York, 1990).
- [34] H. Mohwald, *Annu. Rev. Phys. Chem.* **41**, 441 (1990).
- [35] M. Born and E. Wolf, *Principles of Optics; Electromagnetic Theory of Propagation, Interference and Diffraction of Light*, 5th ed. (Pergamon Press, New York, 1975).
- [36] J. D. Jackson, *Classical Electrodynamics*, 3rd ed. (John Wiley & Sons, Inc., New York, 1999).
- [37] C.-K. Kim, in *Charge-coupled Devices and Systems*, edited by M. J. Howes and D. V. Morgan (John Wiley & Sons, New York, 1979), pp. 1–80.
- [38] G. Bokinsky, D. Rueda, V. K. Misra, A. Gordus, M. M. Rhodes, H. P. Babcock, N. G. Walter, and X. Zhuang, *Proc. Natl. Acad. Sci. U.S.A.* **100**, 9302 (2003).
- [39] X. Zhuang, H. Kim, M. Pereira, H. Babcock, N. Walter, and S. Chu, *Science* **296**, 1473 (2002).
- [40] H. P. Lu, L. Xun, and X. S. Xie, *Science* **282**, 1877 (1998).
- [41] X.-H. Xu and E. S. Yeung, *Science* **275**, 1106 (1997).
- [42] J. J. Macklin, J. K. Trautman, T. D. Harris, and L. E. Brus, *Science* **272**, 255 (1996).
- [43] P. Horowitz and W. Hill, *The Art of Electronics* (Cambridge University Press, Cambridge, 1980).
- [44] L. D. Landau and E. M. Lifshitz, *Fluid Mechanics* (translated from the Russian by J. B. Sykes and W. H. Reid) (Addison-Wesley, London, 1959).